Experimental and modeling study of nitric oxide formation in premixed methanol + air flames

Brackmann, Christian; Methling, Torsten; Lubrano Lavadera, Marco; Capriolo, Gianluca; Konnov, Alexander A.

Published in:
Combustion and Flame

DOI:
10.1016/j.combustflame.2019.11.043

2020

Document Version:
Publisher's PDF, also known as Version of record

Combustion and Flame 213 (2020) 322–330

Contents lists available at ScienceDirect

Combustion and Flame

journal homepage: www.elsevier.com/locate/combustflame

Experimental and modeling study of nitric oxide formation in premixed methanol + air flames

Christian Brackmann*, Torsten Methling, Marco Lubrano Lavadera, Gianluca Capriolo, Alexander A Konnov

Division of Combustion Physics, Lund University, Box 118, SE-221 00 Lund, Sweden

ARTICLE INFO

Article history:
Received 30 August 2019
Revised 5 October 2019
Accepted 28 November 2019
Available online 19 December 2019

Keywords:
Methanol
Flames
NO
LIF
Modeling

ABSTRACT

Validation and further development of models for alcohol combustion requires accurate experimental data obtained under well-controlled conditions. To this end, measurements of nitric oxide, NO, mole fractions in premixed laminar methanol + air flames have been performed using saturated laser-induced fluorescence, LIF. The methanol flames have been stabilized at atmospheric pressure and initial gas temperature of 318 K at equivalence ratios ϕ = 0.7–1.5 using the heat flux method that allows for simultaneous determination of their laminar burning velocity. The LIF signal is converted into NO mole fraction via calibration measurements, which have been performed in flames of methane, methanol and syngas seeded with known amounts of NO. The experimental approach is verified by the measurements of NO mole fractions in the post flame zone of methane flames, investigated in previous studies at similar conditions. Data on the NO formation together with burning velocities for methanol and methane obtained under adiabatic flame conditions provide highly valuable input for model validation. They have been compared with predictions of six different chemical kinetic mechanisms. Summarizing the behavior of all models tested with respect to burning velocities and NO formation in flames of methane and methanol, the mechanism of Glarborg et al. (2018) and the San Diego mechanism (2019) demonstrate uniformly satisfactory performance.

1. Introduction

For the transition of our global energy supply from fossil to renewable sources, fuels are often substituted by biogenic alcohols. To support this transition, chemical kinetic models of alcohol combustion have constantly been improved over recent years [1]. Macroscopic combustion characteristics such as laminar burning velocities or ignition delay times are primary targets for model validation [1,2]. For the simplest alcohol, methanol, Christensen et al. [2] developed a new detailed kinetic mechanism using also experimental data on stable species profiles obtained in shock tubes, low-pressure flames, and in flow- and well-stirred reactors. Additional constraints for the model validation could be imposed using experimental data on NO_x formation in flames. Indeed, quantitative prediction of the nitric oxide, NO, production and consumption in flames of different stoichiometry relies on accurate modeling of concentration profiles of several key radicals, e.g. CH, O, OH, etc. [3]. Detailed understanding of these processes is equally important for optimization and improved design of clean combustion systems, therefore, the formation of NO for C_1–C_4 alcohol fuels has been investigated in several comparative studies with alkanes that included experiments as well as numerical modeling [4–8].

The first study of NO formation in methanol flames has been performed by Li and Williams [4], who employed probe sampling from two-stage flames and demonstrated very good agreement between their rather limited set of experimental data and model predictions. Watson et al. [7,8] investigated C_1–C_4 alcohols in premixed flames arranged in a stagnation-plane burner configuration and measured NO profiles using laser-induced fluorescence, LIF. In their study, stoichiometric flames showed a lower formation of thermal NO for alcohol fuels compared with alkane fuels of corresponding carbon chain length due to reduced flame temperatures. At fuel-rich conditions, NO is also formed via the prompt formation route involving reactions with CH-species, primarily

* Corresponding author.
E-mail address: christian.brackmann@forbrf.lth.se (C. Brackmann).

https://doi.org/10.1016/j.combustflame.2019.11.043

the CH radical. For fuel-rich conditions of equivalence ratio ϕ=1.3, Watson et al. observed lower amounts of NO produced via the prompt formation mechanism for alcohols compared with the corresponding alkane fuel, attributed to reduced formation of CH species [7,8]. Nevertheless, the difference becomes smaller with increasing length of the fuel carbon chains as the relative impact of the alcohol OH group is reduced [8]. Model predictions of NO for methanol was good for most investigated mechanisms at stoichiometry while a tendency to under-prediction was observed at fuel-rich ϕ=1.3 conditions. It was also noted that different models yield somewhat different spatial profiles of temperature, velocity and concentrations of NO and CH that hampers direct comparison with the stagnation-plane-burner experiments. Formation of non-thermal NO in alcohol combustion has also been investigated by Bohon et al. with post-flame probe sampling above a McKenna burner [6] as well as laser-based measurements of NO profiles above the same burner and in Bunsen-type flames [5]. Similar to the results of Watson et al. [7], combustion at fuel-rich conditions showed reduced levels of non-thermal NO for alcohols compared with alkanes [6]. Moreover, reduced consumption of NO via the NO–HCN reburn mechanism was identified [6]. In a follow-up study, where non-thermal NO formation was analyzed and classified into hydrocarbon and non-hydrocarbon sub-mechanisms, a significant contribution to non-thermal NO from non-hydrocarbon routes was identified at fuel-rich conditions [5]. A comparison with the experiments performed in the burner-stabilized flames required measurement of the temperature profiles (e.g., by thermocouples) that introduced additional uncertainties in the data analysis [6].

Laminar premixed flat flames stabilized using the heat flux method facilitate direct comparison with model predictions since they are adiabatic with respect to the burner, have negligible stretch and possess only downstream heat losses which can be evaluated experimentally [9]. Therefore, several studies on NO formation in flames of different hydrocarbons have been performed using probe sampling, e.g. [9–11]. Possible concerns of the intrusive character of probe sampling affecting NO concentration measurements have been dismissed in an independent study of Sepman et al. [12] and then on the same heat flux burner using LIF [13]. Non-intrusive LIF measurements of NO have been reported for a range of fuels in flames under different experimental conditions, see, e.g. [14]. Quantitative NO concentrations are obtained through calibration, either versus Rayleigh scattering or the LIF signal measured in a flame seeded with known amounts of NO. The latter standard-addition technique has, for example, been employed in studies of NO formation in low-pressure CH_4 and C_2H_2 flames [15] as well as in atmospheric-pressure flames of methane [16,17], syngas [18] and alcohols [5,7,8,19].

Different strategies for quantitative measurements of NO using LIF have been employed in our previous studies, e.g. [13,20–23]. In the present work, a LIF installation for NO measurements using the standard-addition technique in flames stabilized using the heat flux method is presented. The objective of this work was to generate new experimental data for modeling purposes. Previously presented laminar burning velocities for methanol + air flames by Vancoillie et al. [24] are augmented with experimental data at fuel-rich conditions for equivalence ratios ϕ= 1.1–1.5. Measurements are made by establishing flames under adiabatic conditions on a heat flux burner. Moreover, LIF is simultaneously employed to measure NO mole fractions in the post flame zone and the experimental approach is verified by measurements in methane flames, investigated in previous studies at similar conditions [9,17,18]. Data on NO formation for methanol thus obtained under adiabatic flame conditions provide highly valuable input for model validation and are compared with predictions of six different chemical kinetic mechanisms.

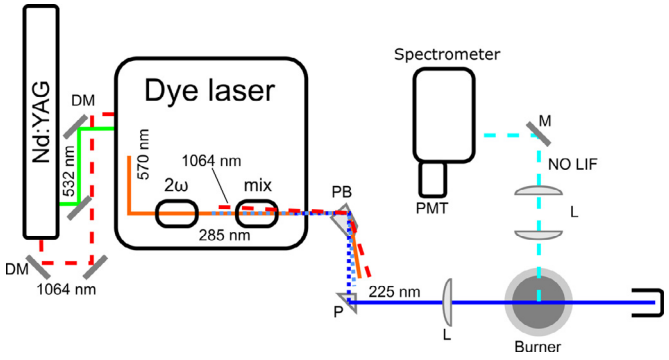

Fig. 1. Schematic of NO LIF setup. Abbreviations: 2ω=doubling crystal, mix=mixing crystal, DM=dichroic mirror, PB=Pellin-Broca prism, P=prism, L=lens, M=mirrors.

2. Experimental details

2.1. Flame stabilization

Adiabatic premixed laminar flames were stabilized at atmospheric pressure on a flat-flame burner through the heat flux method [25], which has been used extensively for measuring laminar burning velocities of gaseous and liquid fuels. A detailed description of the method and associated experimental uncertainties have been presented by Alekseev et al. [26]. The heat flux burner is made of brass with a plate, 30 mm in diameter and 2 mm thick, perforated with small holes (0.5 mm in diameter) attached to the burner outlet. The plate is maintained at a constant temperature, 368 K, by a heating jacket supplied with thermostatic water attached to the burner head. The plenum chamber has a separate heating system, also supplied with water, which sets the initial temperature (T_0) of the fresh gas mixture which was fixed to 298 K and 318 K for methane and methanol, respectively. A mixing panel provides controlled flows of vaporized fuel and air to set the required equivalence ratio. The liquid fuel flow from the fuel reservoir, pressurized by nitrogen, is measured by a liquid mass flow controller (Cori-Flow, Bronkhorst High-Tech) and fed to a Controlled Evaporator Mixer (Bronkhorst High-Tech). The required air flow, controlled by a calibrated gas mass flow controller, is also used as a carrier gas to facilitate vaporization. Neat liquid methanol fuel was used as delivered from Merck in sealed bottles.

For methanol flames, the laminar burning velocity was measured by varying the velocity of the unburned gas until a flat radial temperature distribution over the burner plate, recorded by eight T-type thermocouples (0.1 mm bare wire diameter), is reached. The measurement procedures and data processing algorithms are described elsewhere [26]. On the other hand, laminar burning velocities for methane flames are taken from the literature.

2.2. Saturated LIF

Laser-induced fluorescence measurements of NO were made by excitation of the $A^2\Sigma^+ \leftarrow X^2\Pi$ (0–0) band and a schematic of the LIF setup is shown in Fig. 1. The 532 nm second harmonic of an Nd:YAG laser (Brilliant B, Quantel) pumped a dye laser (Quantel TDL-90) operated on a Rhodamine 590/610 dye mixture. Frequency-doubling of the dye laser output beam followed by frequency mixing with the fundamental beam of the Nd:YAG laser at wavelength 1064 nm provided ultraviolet wavelengths for NO excitation. The laser was tuned to the rather temperature-insensitive

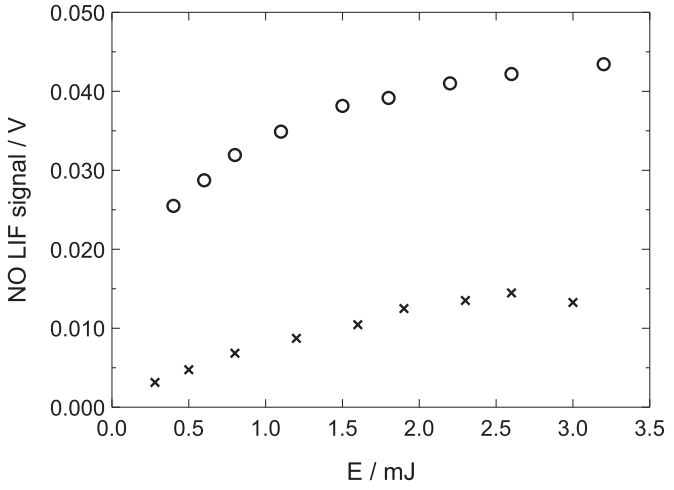

Fig. 2. NO LIF (circles) and off-resonance background (crosses) signals versus laser pulse energy.

$Q_2(26.5)$ NO transition at wavelength 225.5 nm in air (a fluorescence excitation spectrum is shown in the Supplementary material). The UV beam had a spectral linewidth of approximately 1 cm^{-1}, determined by the linewidth of the Nd:YAG laser, and the pulse energy was 2.5–3 mJ. To improve focusing the UV beam was expanded using a telescope arranged with lenses of focal length f=−150 mm and f=+300 mm. A prism directed the expanded beam across the center of the burner surface at height 10 mm and an f=+500 mm spherical lens focused the beam above the burner center.

The NO fluorescence was collected using an arrangement of two spherical lenses with focal lengths f=+150 mm and f=+300 mm, by which the measurement volume was imaged on the slit of a spectrometer (Shamrock SR-500i-A-R, Andor). Two aluminum mirrors were used to image the horizontal laser beam along the vertical spectrometer slit. A longpass filter (LP02-224R-25, Semrock) was used for suppression of background such as flame luminescence and residual scattered laser light. The signal was detected by a photomultiplier tube (model H9305-01, Hamamatsu) mounted at the spectrometer exit. An additional slit was mounted at the spectrometer exit to further filter the signal and detect the (0–1) γ-band of the $A^2\Sigma^+ \rightarrow X^2\Pi$ NO transition, centered at wavelength 236 nm. The photomultiplier signal was registered by a digital oscilloscope (Wavejet Touch 354, Lecroy) and fluorescence signal traces were collected by averaging over 128 laser pulses. In addition to measurements made with the laser tuned to the $Q_2(26.5)$ resonance, corresponding data were recorded with the laser tuned to wavelength 225.38 nm in air, which is off NO resonance. An observed background contribution for NO LIF measurements is laser-induced fluorescence of hot O_2, which has absorption lines in the same spectral region as NO. Even though the $Q_2(26.5)$ transition of NO does not overlap with a strong O_2 transition, there is nevertheless a potential additional LIF background for lean flames, which is corrected for by the off-resonance measurement. The background thus measured at the off-resonance wavelength position was subtracted from the corresponding measurement made on the $Q_2(26.5)$ resonance. The peak value after background subtraction was retrieved for further data evaluation.

In general, NO LIF signals follow a linear dependence on laser irradiance at low irradiances whereas a saturated signal, independent on laser irradiance, is approached at higher values. This is demonstrated in Fig. 2 showing measured NO LIF and off-resonance background signals versus laser pulse energy. At energies higher than ~1.5 mJ the signal shows a weaker dependence on energy and approaches a saturated condition. The signal increase still observed at pulse energies above 1.5 mJ can be due to that excitation partially occurs in the linear regime, for example at the wings of the spatial laser profile where the irradiance is low, and saturation is not fully achieved. For LIF excitation in the linear regime, the fluorescence quantum yield is determined by non-radiative de-excitation due to collisional quenching, which must be considered in the evaluation of quantitative mole fractions. In contrast, at saturated conditions, laser-induced de-population of the energy level in the excited state reduces the impact of quenching and facilitates quantification. To achieve a high degree of saturation in the present setup, measurements were made at pulse energies around 2.5 mJ.

Following excitation of the $Q_2(26.5)$ transition, rotational-energy transfer (RET) in the excited state results in redistribution of the population to other rotational energy levels. For broadband detection of an entire vibrational band, as employed in this study, fluorescence is then obtained from the entire manifold of rotational energy levels. The fluorescence signal is therefore dependent on the RET as transitions from different rotational energy levels have different coefficients of spontaneous emission. In addition, for rotational levels other than the one excited by the laser there is no laser-induced de-population process but only emission of fluorescence and collisional quenching. Thus, the fluorescence yield is under the present experimental conditions determined by RET as well as quenching which need to be considered in data evaluation, following an approach for example reported by Reisel et al. [27] and Ravikrishna et al. [28]. Since it is necessary to consider collisional quenching, quenching-dependent signal contributions due to laser wing effects should be handled appropriately in the data evaluation.

2.3. NO calibration

The LIF signal is converted into NO mole fraction via calibration measurements, in which the signal is measured for different levels of NO seeding in a fuel-lean flame with a very low level of native NO formed. Figure 3(a) shows results from such calibration measurements in flames of equivalence ratio ϕ= 0.7 for methane, syngas (25.5%$_{vol}$ H_2/4.5%$_{vol}$ CO/70%$_{vol}$ N_2) and methanol as well as a ϕ= 0.5 syngas (85% $_{vol}$ H_2 / 15% $_{vol}$ CO) flame. The signal for the methane flame follows a linear trend up to a NO seeding level of 50 ppm and then shows a weaker dependence at higher mole fractions. Data from the syngas flames continue to follow a linear dependence up to the highest level of NO seeding for those flames, 76–77 ppm.

The slopes of the linear trends represent the LIF signal per NO molecule but differ between the data sets and are for example 0.000994 and 0.001528 for the ϕ= 0.7 flames of methane and syngas, respectively. The LIF signal is dependent on the gas number density and thus affected by the flame temperature, which is 1785 K for methane and 1543 K for syngas. The lower temperature of the syngas flame, therefore, results in a 23% higher number density, which gives a higher slope as observed in Fig. 3(a). However, correction for the temperature difference does not fully compensate for the observed difference in slopes. The signal is apparently also dependent on other flame conditions and, as mentioned previously, it was required to also compensate for the influence of collisional quenching to obtain data following similar linear trends. These corrected data sets are presented in Fig. 3(b) and clearly show a similar dependence on NO seeding. Following the discussions in [27,28] RET should also be considered in a detailed analysis. However, Reisel et al. [27] report the distribution of population among rotational levels in the excited state, i.e. the RET, to be similar for different C_2H_6 flames investigated. In addition, Ravikrishna et al. report broadband LIF measurements to be essentially independent of RET effects [28]. Since the slopes

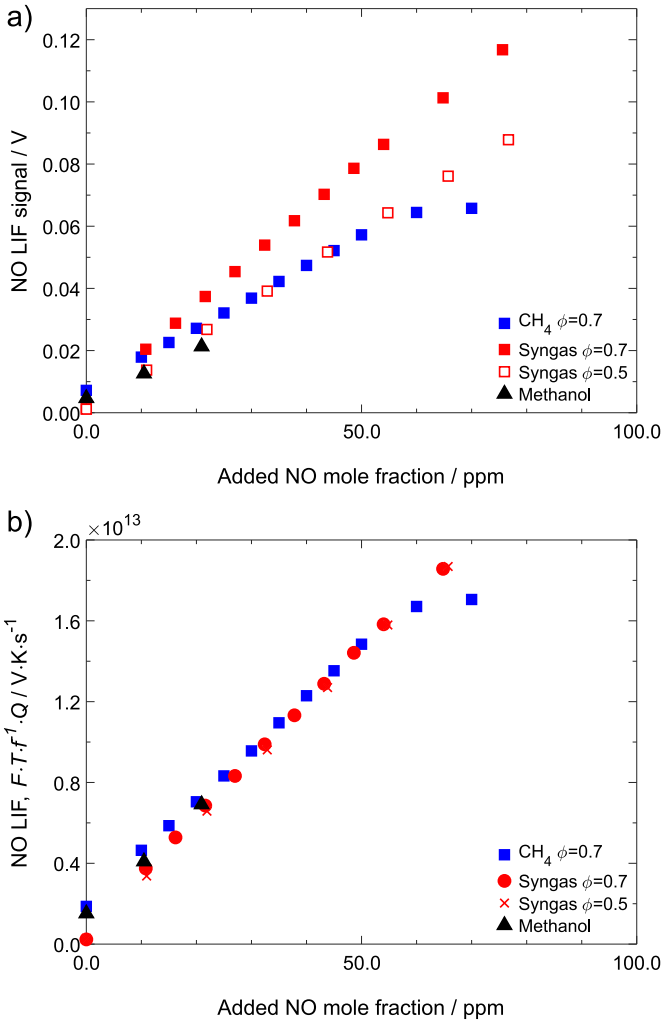

Fig. 3. (a) LIF signal versus NO seeding measured in lean $\phi = 0.7$ flames of methane, syngas (25.5% H_2/4.5% CO/70% N_2) and methanol as well as a ϕ= 0.5 syngas (85% H_2/ 15%CO) flame. (b) LIF signals after corrections for flame temperature and collisional quenching.

of the quenching-corrected data sets in Fig. 3(b), obtained without considering RET, are consistent within 8.7%, the uncertainty due to differences in RET is expected to be within this range. The consistency of 8.7% is assumed to represent the experimental accuracy of the NO quantification procedure since calibration measurements in the different flames provide a combination of calibration, temperature and composition (thus RET and quenching) uncertainties. Each data point in Fig. 3(b) is averaged from 3 or 4 acquisitions for which the experimental repeatability was good with a variance well within the uncertainty given above.

From the graphs of Fig. 3 the fluorescence signal shows a linear dependence on NO seeding and the slope obtained from a linear fit of the data gives a conversion factor between NO signal and mole fraction. The fluorescence signal measured in a flame can be expressed according to Eq. (1)

$$F = C \cdot N_{\mathrm{tot}} \cdot X_{\mathrm{NO}} \cdot f \cdot \frac{1}{Q} \tag{1}$$

where C is a constant of proportionality, f the fraction of NO molecules in the probed energy level, N_{tot} the total gas number density, X_{NO} the NO mole fraction, and Q the collisional quenching rate.

Using Eq. (1) with the quantities above and temperature T for a calibration flame and another flame indicated by subscripts *cal* and *flame*, respectively, the NO mole fraction of the investigated flame can be expressed according to Eq. (2)

$$X_{\mathrm{NO}} = \left(\frac{\Delta X_{NO}}{\Delta F_{NO}}\right)_{cal} \cdot \frac{T_{flame}}{T_{cal}} \cdot \frac{f_{cal}}{f_{flame}} \cdot \frac{Q_{flame}}{Q_{cal}} \cdot F_{flame} \tag{2}$$

where the factor $(\Delta X_{\mathrm{NO}}/\Delta F_{\mathrm{NO}})_{\mathrm{cal}}$ is the reciprocal of the slope of the measured calibration curve (cf. Fig. 3(a)). The NO mole fractions presented in this paper have been evaluated by calibration versus signals measured in a syngas flame, which will be discussed further in the following. According to Eqs. (1) and (2), evaluation of NO mole fractions requires knowledge of temperatures, population fractions, and collisional quenching rates. The flames stabilized on the heat flux burner are ideally assumed to burn under adiabatic conditions with respect to the burner. However, radiative heat losses – mainly from hot H_2O and CO_2 – are present in the post flame zone. Thus, temperatures above the burner were taken from the flame simulations, which included these radiative heat losses. Typically, these calculated temperatures at a position 10 mm above the burner are about 40–70 K lower than the adiabatic temperatures, depending on the equivalence ratio. Numerical computations have shown that this effect has no significant influence on the laminar burning velocity. Population fractions for these temperatures, determined by the Boltzmann distribution, were obtained from the LIFBASE software [29]. Collisional quenching rates were calculated using product-zone concentrations of N_2, O_2, H_2O, and CO_2 obtained from simulations together with collisional quenching cross-sections presented by Settersten et al. [30]. Following the previous discussion on the data of Fig. 3, the impact of RET has not been considered in the evaluation based on Eqs. (1) and (2). With this approach RET is implicitly assumed to be the same for all flames investigated. The LIF calibration and evaluation have been analyzed in terms of uncertainties due to possible overlap with neighboring NO transitions, temperature and collisional quenching. Results and discussion on these topics are presented in the Supplementary material.

The calibration in flames of different fuels described above was also aimed at elucidation of a possible effect of NO reburning in calibration flames. It is commonly assumed that a small amount of NO (e.g., <100 ppm) seeded into a lean flame does not react (within 10%), e.g. [19,28]. This assumption was put forward by Reisel et al. [27] and substantiated by numerical modeling using different mechanisms. However, in the LIF study of Schultz et al. [31] consumption of NO was observed for atmospheric and high-pressure methane and n-heptane flames. Also, probe sampling measurements in flames of methane [10] and other hydrocarbons (C_2H_4, C_2H_6, C_3H_8) [11] seeded with NO demonstrated reburning in lean mixtures as well. Possible reburning decreases apparent slopes of the calibration plots as illustrated in Fig. S6 of the Supplementary material comparing lean, stoichiometric, and fuel-rich methane flames. Moreover, it is expected that reburning by non-hydrocarbon fuels, such as syngas, should be less effective compared to hydrocarbons [32]. Careful analysis of the calibration dependencies shown in Fig. 3(b) indeed show that the slopes for syngas flames are somewhat higher than for methane and methanol flames. Therefore, calibration slopes obtained in syngas flames have been used in the following data processing.

3. Numerical modeling

The flames on the heat flux burner were simulated using the open-source software Cantera [33] with the one-dimensional FreeFlame model. Thermodiffusion, multicomponent diffusion and radiative heat losses were all considered in the simulations. The radiation model considers the radiation from CO_2 and H_2O through an optically thin medium (particle radiation is not considered for the investigated, non-sooting flames). Especially, the radiative heat

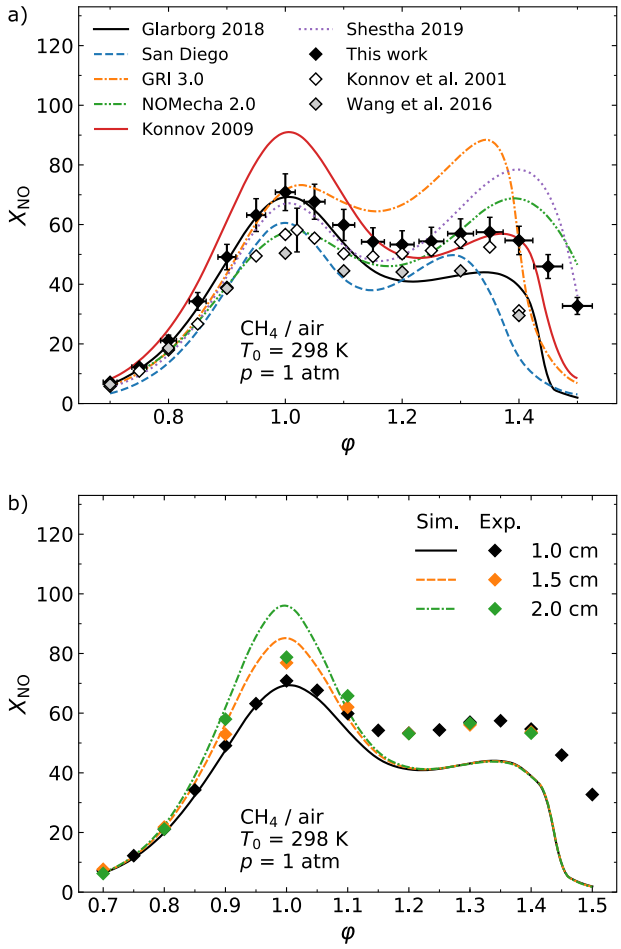

Fig. 4. (a) Experimental and numerical NO mole fractions at HAB=10 mm for methane + air flames. Experimental data are from the present work and [9,18] while models include Glarborg 2018 [3], San Diego [34], GRI 3.0 [35], NOMecha 2.0 [15], Konnov 2009 [36], and Shrestha 2019 [37]. (b) Measured NO mole fractions for methane + air flames at different heights above the burner compared with simulation results obtained with the Glarborg model [3].

losses have a significant influence on the simulated results for the formation of thermal NO [9]. The simulation convergence thresholds of the gradient and curvature fractional change of neighboring grid points were both set to 0.1. To shift the simulated distances of the free flame to corresponding heights above the burner (HAB), the point of HAB=0 mm was set to the point where the surface plate temperature was reached. Simulations were made using the following chemical kinetic mechanisms to assess their performance: Glarborg 2018 [3], San Diego [34], NOMecha 2.0 [15], GRI 3.0 [35] and Konnov 2009 [36]. For the San Diego model, we selected the latest hydrocarbon model from December 2016 and the revised version of the NO sub-model from 2004 [34]. All these models are general-purpose kinetic schemes mostly developed and validated for methane, however, they automatically include a methanol combustion sub-mechanism. Moreover, Shrestha et al. [37] recently developed a dedicated model for methanol and ethanol oxidation, which was also tested here.

4. Results and discussion

Figure 4(a) shows experimental and calculated NO mole fractions at HAB=10 mm in methane + air flames. Two different zones can be identified in the profiles where the obtained mole fraction is dominated by two different main formation routes of NO. Around stoichiometric conditions the highest adiabatic temperatures are reached and most NO under these combustion conditions is formed via the thermal pathway [3,9]. At fuel-rich conditions, a second NO peak can be identified in the profiles and this NO typically stems from the prompt NO pathway, which is mainly caused by CH radicals appearing in significant amounts at fuel-rich conditions [3,9]. Figure 4(b) shows NO mole fraction measured at heights 10, 15 and 20 mm above the burner together with predictions of the Glarborg mechanism. For flames of equivalence ratios ϕ=0.9–1.1, NO mole fractions at 15 and 20 mm are up to ~10 ppm higher than at height 10 mm due to higher amounts of thermal NO produced for these flames [9]. In contrast, for fuel-rich flames of $\phi > 1.1$ where the formation of NO via the prompt mechanism dominates, the NO mole fractions at the different heights are the same. The observed trends are reproduced by modeling, as demonstrated for predictions by the Glarborg mechanism, shown with solid lines in Fig. 4(b). However, at the stoichiometric condition, the model overestimates the NO mole fraction above 10 mm height. Since the NO production in the hot post flame zone at stoichiometric conditions is attributed to the thermal NO formation, the differences could be caused by temperature variations between the experimental and simulated flows. Temperature differences might be caused, e.g., by flow entrainment from the ambient air or convective heat losses, which are both neglected by the simulation model. Moreover, in the 1D modeling radial radiation losses are neglected, which in the experiment may be non-negligible due to finite burner size. Nevertheless, the small differences in the NO mole fraction between different heights suggest that an uncertainty in the measurement position on the order of 1 mm should have little influence on the measured mole fractions.

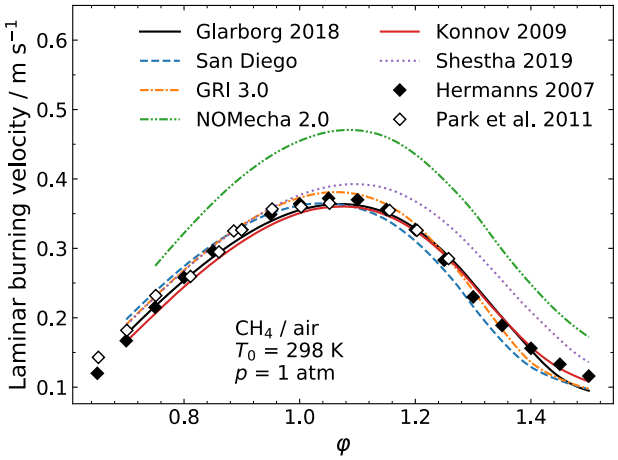

Fig. 5. Experimental and numerical laminar burning velocities for methane + air mixtures. Experimental data are from [38,39] and models are Glarborg 2018 [3], San Diego [34], GRI 3.0 [35], NOMecha 2.0 [15], Konnov 2009 [36] and Shrestha 2019 [37].

Differences can be seen between the probe measurements of Konnov et al. [9] and the LIF measurements in this work around the stoichiometric condition and for very fuel-rich conditions (Fig. 4(a)). The main reason for the differences is most likely the disturbance of the flow and temperature field by the invasive probe, compared to the non-intrusive LIF method. For very fuel-rich conditions, the heat flux burner flames become less stable and flow rates become smaller, due to the lower laminar burning velocities (Fig. 5). As a consequence, the disturbance on the flame stabilization by the probe is more stressed. Additionally, due to the low flow rates of the burner the impact of entrained air caused by the suction of the probe is also pronounced, diluting the probed NO. Introducing a probe into the flame around stoichiometric conditions, where the highest temperatures are reached and most thermal NO is produced [9], will decrease temperatures and reduce the

formation of thermal NO. This would explain the lower NO mole fractions obtained by the probe measurements compared with the LIF measurements around stoichiometric conditions. The explanation is backed by the fact that probe and LIF measurements agree very well at fuel-rich conditions around ϕ=1.15–1.35. At these conditions the main production of NO is via the prompt NO route and the contribution of thermal NO is significantly lower [9]. Since prompt NO is formed in the flame zone, and measurements are taken in the post flame zone, the probe effect on the measurements is much lower compared to the stoichiometric case. In summary, the LIF setup for quantitative NO measurements is well verified by the comparison with the probe measurement and the identification of the reasons for the partial differences.

Profiles of NO mole fractions versus equivalence ratio of methane + air flames have been presented by Wang et al. [18] for a heat flux burner arranged in an experimental setup similar to the one presented in this work. The values obtained by Wang et al. [18] are lower than the results obtained in the present study (cf. Fig. 4(a)), typically by 20% at fuel-rich conditions, and also deviate from the results presented by Konnov et al. [9]. The evaluated results are strongly dependent on correct background subtraction and while Wang et al. [18] do not give any specific details on background subtraction on and off NO resonance in their paper, this could be a source of the observed differences. In addition, collisional quenching is neglected in the analysis presented in [18], however, recalculation of their results taking quenching into account only resulted in a small adjustment of the data. Furthermore, the modeling approach of the heat losses in the flame is different between this study and the work of Wang et al. [18] where an empirical temperature decrease of 100 K/cm suggested by Konnov et al. [9] is assumed. In this study, however, the heat loss is directly computed in the solver implemented in Cantera, by assuming the radiation losses of hot CO_2 and H_2O through an optically thin medium [33]. This approach results in temperature decreases comparable to the assumption of 100 K/cm at low flow speeds. At higher flow speeds, however, the assumed temperature decay is over predicted compared to the simulated solution (see Fig. S7 in Supplementary materials). For further comparison, the value of 57 ppm measured in this study for the ϕ=1.3 flame was also obtained by Watson et al. from NO LIF measurements in the post-flame region of a close-to-adiabatic ϕ=1.3 methane + air flame [7].

All models presented in Fig. 4(a) capture the general trends for NO formation in the thermal zone around stoichiometric conditions and the prompt zone for fuel-rich conditions. However, none of the models is capable to fully reproduce the measured NO mole fractions in the methane flames. The simulation results of the NOMecha 2.0 model show relatively good agreement with the experimental NO mole fractions in Fig. 4(a), but the model significantly over predicts the laminar burning velocities, as shown in Fig. 5. Consequently, the residence time of the fluid in the simulation is shorter than the experimental conditions. Since the production of NO is similar to the experimental data in near-stoichiometric flames, the production rate of thermal NO must be too high to achieve this amount at shortened residence time.

Figure 6 shows the comparison between experimental and numerical results for NO mole fractions at HAB=10 mm in methanol flames. Similar to the methane flames, thermal NO is mostly formed around stoichiometric conditions. Contrary to the methane flames, the formation of prompt NO at fuel-rich conditions is not prominent. The reason can be found in the oxidation pathways of methanol and methane. Methane is consumed via the methyl radical CH_3, which will subsequently form CH radicals during the combustion process, promoting prompt NO. In contrast, methanol is mainly consumed via CH_2OH, CH_2O, HCO to CO, CO_2, and H_2O [6]. Thereby, negligible contents of CH radicals are formed in the combustion process. The experimental NO mole fraction of 14 ppm ob-

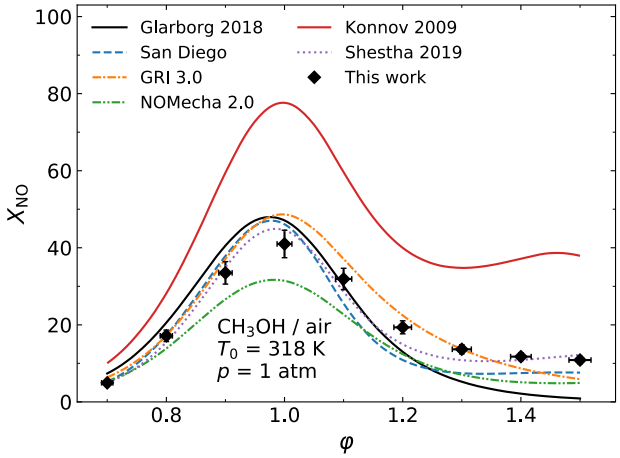

Fig. 6. Experimental and numerical NO mole fractions at HAB=10 mm for methanol + air flames. Models include Glarborg 2018 [3], San Diego [34], GRI 3.0 [35], NOMecha 2.0 [15], Konnov 2009 [36] and Shrestha 2019 [37].

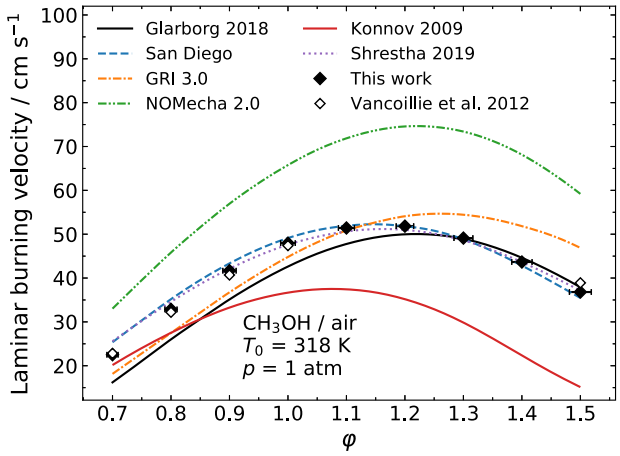

Fig. 7. Laminar burning velocities of methanol + air mixtures. Experiments: present study and [24]. Models are Glarborg 2018 [3], San Diego [34], GRI 3.0 [35], NOMecha 2.0 [15], Konnov 2009 [36] and Shrestha 2019 [37].

tained for the ϕ=1.3 flame is in very good agreement with a value of 13 ppm obtained for a methanol-air flame in the investigation by Watson et al. [7].

Overall, the models Glarborg 2018, San Diego and GRI 3.0 are in good agreement with the experimental values of the NO mole fractions in the post flame zone. The NOMecha 2.0 and Konnov 2009 models, under and over predicts the thermal NO production, respectively. The reason for these deviations can be explained by the model predictions of the laminar burning velocities shown in Fig. 7. The models NOMecha 2.0 and Konnov 2009 over predict and under predict the burning velocities, respectively. Therefore, the residence times of the fluid between the HAB of 0 mm and 10 mm are decreased or increased, respectively. This leads to corresponding changes in the formation of thermal NO, which is highly dependent on these time scales.

Altogether, only the Glarborg [3] and San Diego [34] mechanisms demonstrate uniformly satisfactory performance for prediction of burning velocities and NO formation in flames of methane and methanol. To investigate the simulation results in terms of NO profiles, sensitivity analyses were performed for both fuels at stoichiometric (maximum NO mole fraction) and fuel-rich (local maximum NO mole fraction) conditions using these two models. Results for CH_4 and CH_3OH are presented in Figs. 8 and 9, respectively. At the stoichiometric conditions the thermal formation of

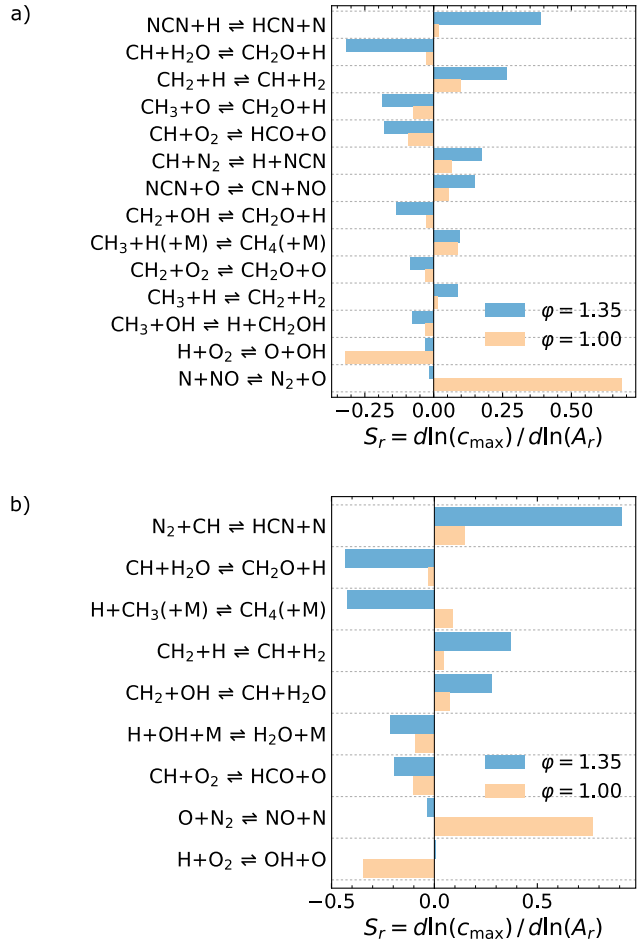

Fig. 8. Sensitivity analysis for the NO mole fractions in methane + air flames, HAB=10 mm, with (a) the Glarborg model [3] and (b): the San Diego model [34].

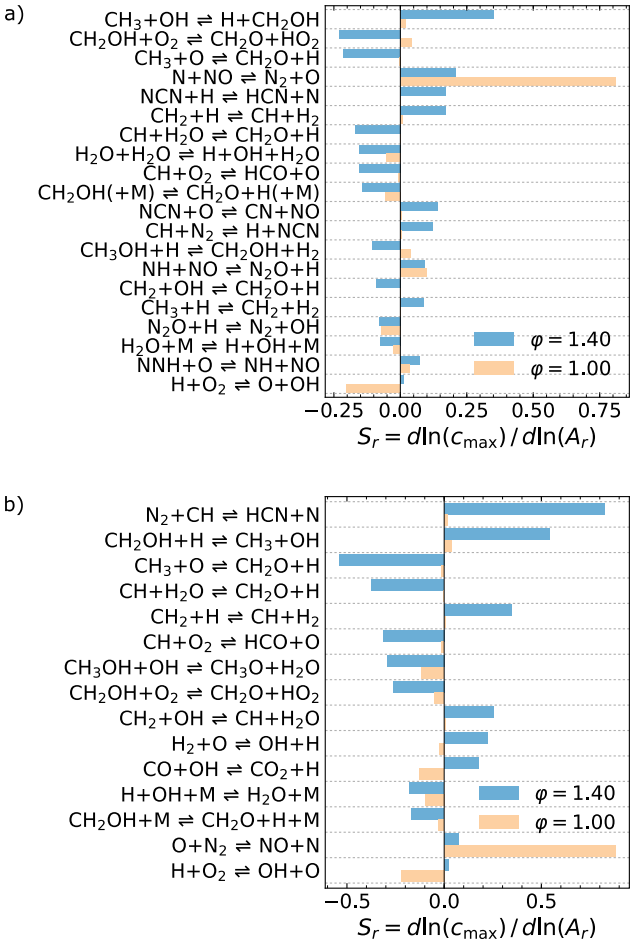

Fig. 9. Sensitivity analysis for the NO mole fractions in methanol + air flames, HAB=10 mm, with (a) the Glarborg model [3] and (b) the San Diego model [34].

NO via N_2 + O ⇔ NO + N has the highest impact on the overall NO formation. This is expected due to the high adiabatic flame temperatures as discussed previously. In addition, reactions H + O_2 ⇔ OH + O and CH_3 + H(+M) ⇔ CH_4(+M) are very sensitive at the stoichiometric conditions because they have a high impact on the heat-release rate in the reaction zone. The other sensitive reactions under stoichiometric conditions can be related to the prompt NO formation.

Under fuel-rich conditions, almost all sensitive reactions in Figs. 8 and 9 are related to prompt NO formation involving the CH radical. The San Diego model is considering CH + N_2 ⇔ HCN + N formation as the initial step in the prompt formation pathway (cf. Fig. 8(b)). Contrary, the newer Glarborg model includes CH + N_2 ⇔ NCN + H as this initial step (cf. Fig. 8(a)) [40]. For the methane combustion, other sensitive reactions for the prompt NO formation are related to the formation and consumption of CH which is mainly formed by triplet methylene CH_2. Also for fuel-rich methanol combustion, the sensitive reactions relate to the formation and consumption of CH (cf. Fig. 9). As illustrated in Fig. 10, pathways are competing, either going through formaldehyde (CH_2O) and subsequent oxidation or via CH_3 and CH_2 to the formation of CH. In conclusion, the sensitive reactions are sensitive because they either promote the CH_2O route reducing the CH formation or promote the CH_3/CH_2 route leading to CH formation.

Overall the differences in the simulation results of the NO mole fractions in fuel-rich flames from the Glarborg model and the San Diego model can be explained by the CH formation, for which simulated spatial profiles are shown in Fig. 11. Here, the San Diego

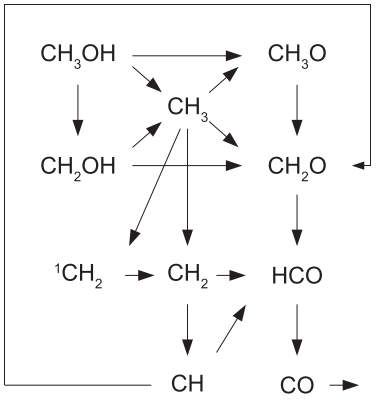

Fig. 10. Simplified reaction pathways for the oxidation of methanol.

model predicts a higher and broader CH profile, compared to the Glarborg model. This is directly leading to enhanced formation of prompt NO with the San Diego model. For both models, the quantity of formation is dominated by the hydrocarbon part of the chemical kinetic model and barely affected by the nitrogen submodel for the formation of prompt NO, which is also illustrated by the rate of production analysis presented in Fig. 12. On the whole, to improve the model predictions towards experimental results, our analysis shows that both the hydrocarbon model of methanol combustion as well as the prompt NO model need to be investigated thoroughly.

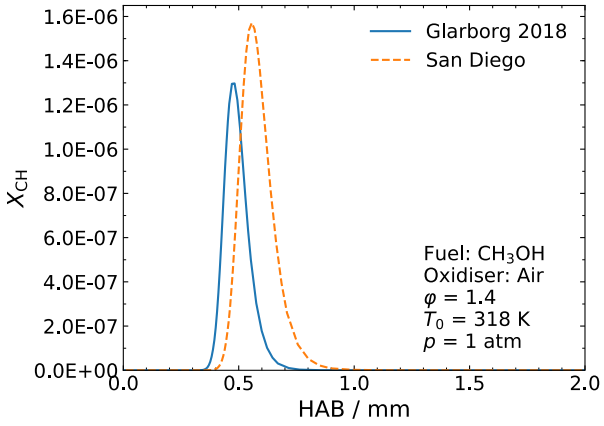

Fig. 11. Simulated CH profiles in fuel-rich ϕ=1.4 methanol + air flame.

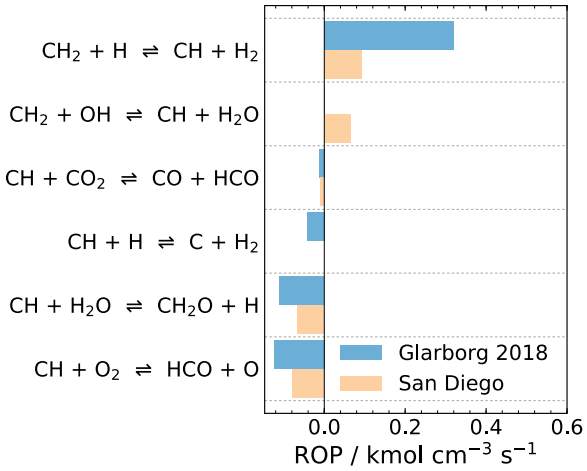

Fig. 12. Rate of production analysis of NO at the position of its maximum mole fraction in fuel-rich ϕ=1.4 methanol + air flame.

5. Conclusions

Important data on laminar burning velocities and post-flame NO mole fractions have been obtained for methanol flames. A method for quantitative NO measurements by the LIF technique has been carefully investigated by calibration measurements under different flame conditions and mole fractions measured in methane flames have been verified by comparison with data from literature. The advantages of the non-invasive LIF measurement technique compared to invasive probe measurements are clearly demonstrated. Altogether, the numerical investigations showed high deviations between the different chemical kinetic model predictions. Therefore, the data obtained within this work are of utmost importance for modelers and will help to improve future chemical kinetic models. Summarizing the behavior of all models tested for prediction of burning velocities and NO formation in flames of methane and methanol, the Glarborg [3] and San Diego [34] mechanisms demonstrate uniformly satisfactory performance. Remarkably, the GRI-mech model [35] optimized for methane and natural gas combustion failed in the prediction of NO formation in fuel-rich methane flames.

Declaration of Competing Interest

The authors declare that they have no known competing financial interests or personal relationships that could have appeared to influence the work reported in this paper.

Acknowledgments

The authors gratefully acknowledge funding support from the Swedish Energy Agency through the project GRECOP (Generic research for optimized energy conversion processes), project number 38913-2; the German Research Foundation (ME 5110/1-1, 397116102); the European Research Council, Advanced Grant TUCLA 669466; the Knut and Alice Wallenberg Foundation, project KAW 2015.0294; the Swedish Research Council, project number 2015-04042.

Supplementary materials

Supplementary material associated with this article can be found, in the online version, at doi:10.1016/j.combustflame.2019.11.043.

References

[1] S.M. Sarathy, P. Osswald, N. Hansen, K. Kohse-Hoinghaus, Alcohol combustion chemistry, Prog. Energy Combust. 44 (2014) 40–102.
[2] M. Christensen, E.J.K. Nilsson, A.A. Konnov, A systematically updated detailed kinetic model for CH_2O and CH_3OH combustion, Energy. Fuel 30 (2016) 6709–6726.
[3] P. Glarborg, J.A. Miller, B. Ruscic, S.J. Klippenstein, Modeling nitrogen chemistry in combustion, Prog. Energy Combust. 67 (2018) 31–68.
[4] S.C. Li, F.A. Williams, Formation of NO_x, CH_4, and C_2 species in laminar methanol flames, 27th Symposium (International) on Combustion, 1 and 2 (1998), pp. 485–493.
[5] M.D. Bohon, T.F. Guiberti, W.L. Roberts, PLIF measurements of non-thermal NO concentrations in alcohol and alkane premixed flames, Combust. Flame 194 (2018) 363–375.
[6] M.D. Bohon, T.F. Guiberti, S.M. Sarathy, W.L. Roberts, Variations in non-thermal NO formation pathways in alcohol flames, Proc. Combust. Inst. 36 (2017) 3995–4002.
[7] G.M.G. Watson, P. Versailles, J.M. Bergthorson, NO formation in premixed flames of C_1–C_3 alkanes and alcohols, Combust. Flame 169 (2016) 242–260.
[8] G.M.G. Watson, P. Versailles, J.M. Bergthorson, NO formation in rich premixed flames of C_1–C_4 alkanes and alcohols, Proc. Combust. Inst. 36 (2017) 627–635.
[9] A.A. Konnov, I.V. Dyakov, J. De Ruyck, Probe sampling measurements and modeling of nitric oxide formation in methane-air flames, Combust. Sci. Technol. 169 (2001) 127–153.
[10] D.A. Knyazkov, A.G. Shmakov, I.V. Dyakov, O.P. Korobeinichev, J. De Ruyck, A.A. Konnov, Formation and destruction of nitric oxide in methane flames doped with NO at atmospheric pressure, Proc. Combust. Inst. 32 (2009) 327–334.
[11] A.A. Konnov, I.V. Dyakov, D.A. Knyazkov, O.P. Korobeinichev, Formation and destruction of nitric oxide in no doped premixed flames of C_2H_4, C_2H_6, and C_3H_8, at atmospheric pressure, Energy Fuel 24 (2010) 4833–4840.
[12] A.V. Sepman, A.V. Mokhov, H.B. Levinsky, The effects of hydrogen addition on NO formation in atmospheric-pressure, fuel-rich-premixed, burner-stabilized methane, ethane and propane flames, Int. J. Hydrogen Energy 36 (2011) 4474–4481.
[13] B. Li, Y. He, Z.S. Li, A.A. Konnov, Measurements of NO concentration in NH_3-doped CH_4 + air flames using saturated laser-induced fluorescence and probe sampling, Combust. Flame 160 (2013) 40–46.
[14] K. Kohse-Höinghaus, J.B. Jeffries, Applied Combustion Diagnostics, Taylor&Francis, New York, 2002.
[15] N. Lamoureux, H.E. Merhubi, L. Pillier, S. de Persis, P. Desgroux, Modeling of NO formation in low pressure premixed flames, Combust Flame 163 (2016) 557–575.
[16] S.V. Naik, N.M. Laurendeau, Laser-saturated and linear laser-induced fluorescence measurements of nitric oxide in counterflow diffusion flames under non-sooting oxygen-enriched conditions, Combust. Sci. Technol. 174 (2002) 1–21.
[17] Y.J. Zhou, Z.H. Wang, Y. He, R. Whiddon, D.X. Xu, Z.S. Li, K.F. Cen, Effects of CH_4 content on no formation in one-dimensional adiabatic flames investigated by saturated laser-induced fluorescence and Chemkin modeling, Energy Fuel 31 (2017) 3154–3163.
[18] Z.H. Wang, Y.J. Zhou, R. Whiddon, Y. He, K.F. Cen, Z.S. Li, Investigation of NO formation in premixed adiabatic laminar flames of H_2/CO syngas and air by saturated laser-induced fluorescence and kinetic modeling, Combust. Flame 164 (2016) 283–293.
[19] C.S.T. Marques, L.G. Barreta, M.E. Sbampato, A.M. dos Santos, Laser-saturated fluorescence of nitric oxide and chemiluminescence measurements in premixed ethanol flames, Exp. Therm. Fluid Sci. 34 (2010) 1142–1150.
[20] C. Brackmann, V.A. Alekseev, B. Zhou, E. Nordstrom, P.E. Bengtsson, Z.S. Li, M. Aldén, A.A. Konnov, Structure of premixed ammonia plus air flames at atmospheric pressure: laser diagnostics and kinetic modeling, Combust. Flame 163 (2016) 370–381.

[21] C. Brackmann, J. Bood, J.D. Nauclér, A.A. Konnov, M. Aldén, Quantitative picosecond laser-induced fluorescence measurements of nitric oxide in flames, Proc. Combust. Inst. 36 (2017) 4533–4540.
[22] C. Brackmann, J.D. Nauclér, S. El-Busaidy, A. Hosseinnia, P.E. Bengtsson, A.A. Konnov, E.J.K. Nilsson, Experimental studies of nitromethane flames and evaluation of kinetic mechanisms, Combust. Flame 190 (2018) 327–336.
[23] C. Brackmann, E.J.K. Nilsson, J.D. Naucler, M. Aldén, A.A. Konnov, Formation of NO and NH in NH_3-doped $CH_4 + N_2 + O_2$ flame: experiments and modelling, Combust. Flame 194 (2018) 278–284.
[24] J. Vancoillie, M. Christensen, E.J.K. Nilsson, S. Verhelst, A.A. Konnov, Temperature dependence of the laminar burning velocity of methanol flames, Energy Fuel 26 (2012) 1557–1564.
[25] K.J. Bosschaart, L.P.H. de Goey, Detailed analysis of the heat flux method for measuring burning velocities, Combust. Flame 132 (2003) 170–180.
[26] V.A. Alekseev, J.D. Naucler, M. Christensen, E.J.K. Nilsson, E.N. Volkov, L.P.H. de Goey, A.A. Konnov, Experimental uncertainties of the heat flux method for measuring burning velocities, Combust. Sci. Technol. 188 (2016) 853–894.
[27] J.R. Reisel, C.D. Carter, N.M. Laurendeau, M.C. Drake, Laser-saturated fluorescence measurements of nitric-oxide in laminar, flat, $C_2H_6/O_2/N_2$ flames at atmospheric-pressure, Combust. Sci. Technol. 91 (1993) 271–295.
[28] R.V. Ravikrishna, C.S. Cooper, N.M. Laurendeau, Comparison of saturated and linear laser-induced fluorescence measurements of nitric oxide in counterflow diffusion flames, Combust. Flame 117 (1999) 810–820.
[29] J. Luque, D.R. Crosley, LIFBASE: Database and spectral simulation (version 1.5), SRI International Report MP 99-009, (1999).
[30] T.B. Settersten, B.D. Patterson, J.A. Gray, Temperature-and species-dependent quenching of NO A $^2\Sigma^+$ (v'=0) probed by two-photon laser-induced fluorescence using a picosecond laser, J. Chem. Phys. 124 (2006) 234308.
[31] C. Schulz, V. Sick, U.E. Meier, J. Heinze, W. Stricker, Quantification of NO A-X(0,2) laser-induced fluorescence: investigation of calibration and collisional influences in high-pressure flames, Appl. Opt. 38 (1999) 1434–1443.
[32] P. Glarborg, P.G. Kristensen, K. Dam-Johansen, M.U. Alzueta, A. Millera, R. Bilbao, Nitric oxide reduction by non-hydrocarbon fuels. implications for reburning with gasification gases, Energy Fuel 14 (2000) 828–838.
[33] D.G. Goodwin, R.L. Speth, H.K. Moffat, B.W. Weber, Cantera: an object-oriented software toolkit for chemical kinetics, thermodynamics, and transport processes. Version 2.4.0., doi:10.5281/zenodo.1174508, 2018.
[34] Chemical-Kinetic Mechanisms for Combustion Applications, San Diego Mechanism web page, Mechanical and Aerospace Engineering (Combustion Research), University of California at San Diego (http://combustion.ucsd.edu), 2019.
[35] G.P. Smith, D.M. Golden, M. Frenklach, N.W. Moriarty, B. Eiteneer, M. Goldenberg, C.T. Bowman, R.K. Hanson, S. Song, W.C.J. Gardiner, V.V. Lissianski, Z. Qin, GRI 3.0 mechanism. http://www.me.berkeley.edu/gri_mech/, 2019.
[36] A.A. Konnov, Implementation of the ncn pathway of prompt-NO formation in the detailed reaction mechanism, Combust. Flame 156 (2009) 2093–2105.
[37] K.P. Shrestha, L. Seidel, T. Zeuch, F. Mauss, Kinetic modeling of NO_x formation and consumption during methanol and ethanol oxidation, Combust. Sci. Technol. 191 (2019) 1628–1660.
[38] I. Dyakov, A.A. K.onnov, J. De Ruyck, K. Bosschaart, E.C.M. Brock, P. Goey, Measurement of adiabatic burning velocity in methane-oxygen-nitrogen mixtures, Combust. Sci. Technol. 172 (2001) 81–96.
[39] O. Park, P.S. Veloo, N. Liu, F.N. Egolfopoulos, Combustion characteristics of alternative gaseous fuels, Proc. Combust. Inst. 33 (2011) 887–894.
[40] L.V. Moskaleva, M.C. Lin, The spin-conserved reaction $CH+N_2$ ->H+NCN: a major pathway to prompt No studied by quantum /statistical theory calculations and kinetic modeling of rate constant, Proc. Combust. Inst. 28 (2000) 2393–2401.